The International Journal of Advanced Manufacturing Technology (2022) 120:7219–7233
https://doi.org/10.1007/s00170-022-09213-0

ORIGINAL ARTICLE

A grinding force prediction model with random distribution of abrasive grains: considering material removal and undeformed chips

Xuezhi Wang[1,2] · QingYao Liu[1,2] · Yaohui Zheng[1,2] · Wei Xing[3] · Minghai Wang[1,2]

Received: 18 October 2021 / Accepted: 10 April 2022 / Published online: 23 April 2022
© The Author(s), under exclusive licence to Springer-Verlag London Ltd., part of Springer Nature 2022

Abstract
Grinding force is an important index for understanding grinding mechanism. In this paper, based on the single grain-grinding experiment, the grinding force under different grinding parameters was studied. Based on the undeformed chip, the grinding force model of multi-grain abrasive was established. Combined with the randomness of grains distribution, the grinding force model was further improved. And the grinding specific energy under different undeformed chip thickness was obtained by single CBN abrasive grain scratch tests. In addition, grinding experiments were carried out under different grinding parameters, and corresponding grinding force was measured. The results show that the grinding specific energy changes with the change of the undeformed chip thickness. For grinding 45 steel with ceramic bond CBN wheel, when the deformation cutting thickness reaches 50 μm, the grinding specific energy tends to 3460 J/mm^3. Under the same grinding parameters, the calculated values of grinding force model are in good agreement with the experimental values. Confirmed by further research, the model has better applicability to small cutting depth, slow feed, and low speed cutting models. This study has certain guiding significance for further research on grinding mechanism and characterizing the grinding force.

Keywords Grinding force · Random distribution · Undeformed chip

1 Introduction

The grinding force is produced by the relative dynamic interference between workpiece and grinding wheel. In the grinding process, the abrasive grains on the surface of the grinding wheel move along a specific trajectory in the shallow layer of the workpiece to achieve material removal. In this process, the workpiece will appear elastic deformation and plastic deformation and finally form the cutting. These are rubbing, ploughing, and cutting as shown in Fig. 1. The grinding force can reflect the basic characteristics of the grinding process. It is not only the most important physical quantity in the grinding process, but also an important index to evaluate the grindability of materials.

In general, grinding force plays an important role in grinding process. It not only directly affects the grinding wheel wear, grinding accuracy, grinding temperature, and surface integrity, but also strongly affects the material removal mechanism [1]. At present, the modeling of grinding force mainly includes two kinds. One method is to predict the grinding force by planning, statistics, neural network, gray prediction, and other methods based on the sample values of grinding force measured in grinding experiments. The other is using kinematic model and mechanical model to establish the mathematical expression of grinding force based on a mass of experimental data [2].

It is very difficult to observe and analyze the grinding process experimentally because of many abrasive grains, irregular geometric shape, and inconsistent grinding depth. In the prediction of experimental grinding force, Huang et al. [3] studied the influence of grinding depth and table speed

✉ Xuezhi Wang
wangxuezhineu@126.com

✉ Minghai Wang
wangminghai2008@163.com

1 School of Mechatronics Engineering, Shenyang Aerospace University, Shenyang, China

2 Key Laboratory of Fundamental Science for National Defense of Aeronautical Digital Manufacturing Process, Shenyang Aerospace University, Shenyang, China

3 Beijing Special Engineering and Design Institute, Beijing, China

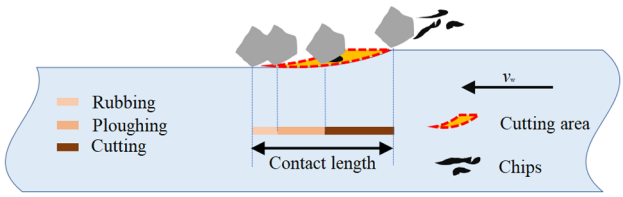

Fig. 1 Three different phases of material deformation modes

on grinding force and grinding force ratio through grinding experiments of SiC particle reinforced aluminum matrix composites (SiCp/Al) under wet, dry, low temperature, and ELID grinding conditions. Fuh and Wang [4] used BP neural network to model and predict the grinding force in creep feed grinding process. Gu et al. [5] measured the grinding forces under different parameters by grinding tests and established the prediction model of grinding force of multi-grain abrasive by using the support vector machine (SVM) prediction method based on particle swarm optimization.

In order to overcome the deficiency of the test model, the mechanism of material removal during grinding was revealed. Most scholars studied the grinding mechanism from the single grain cutting and then predicting the grinding force [6–9]. Hecker et al. [10, 11] deduced the calculation expression of undeformed chip thickness by assuming that the grinding particle height follows Rayleigh distribution, and established the prediction model of grinding force based on the definition of hardness test. Liu et al. [12] utilized the single-grain simulation to investigate the individual crack generation and propagation in silicon carbide (SiC). Xie et al. [13] established a mathematical model of high speed deep grinding force of engineering ceramics based on the grinding force of a single grain. Shao et al. [14] presented a predictive modeling of MQL grinding force through considerations of boundary lubrication condition by extrapolating the single grain interaction to the whole wheel. Zhang et al. [15, 16] presented an improved theoretical force model that considered material-removal and plastic-stacking mechanisms. Cheng et al. [17] established a model of the micro drill-grinding force by using a physical method based on the undeformed chip thickness. Zhang et al. presented a theoretical grinding force model by the consideration of the ductile stage, the ductile-to-brittle-transition-stage, and the brittle stage and used the model to predict the grinding force of zirconia ceramic [18]. Li et al. [19] proposed an analytical model from the microscopic perspective. In addition, many scholars have studied the ultrasonic assisted grinding force model [20, 21].

These studies always ignored the abrasive distribution on the grinding wheel, and the influence of the difference in abrasive size on the removal mode for grinding force [22–24]. In addition, most of the previous studies based on the average cutting depth or average chip thickness model, but not based on the grinding process model, can only be used to predict the average grinding force [19].

The size and variation of grinding force are not only related to the characteristics and machining parameters of the grinding wheel, but also closely related to the properties and microstructure of the material itself. In this paper, a grinding force prediction model of multi-grain abrasive was established. And it will be beneficial to achieve effective prediction grinding force in the establishment of grinding force model. Besides, the error between the theoretical value and the experimental value will be reduced as well. To sum up, this research has certain engineering practical significance for further study.

2 Review of research

2.1 Grinding force model based on dynamic cutting edge

The grinding edges are the cutting entity. They are randomly distributed on the surface of the grinding wheel. The spacing of abrasive grains and their respective protruding heights are different. And in the process of grinding, part of the lower grinding abrasive grains will not be able to participate in cutting. As a result, the actual number of grains involved in cutting will be less than the actual number of grains on the surface of the grinding wheel. From whether to participate in the cutting, the grinding edges can be divided into static effective grinding edge and dynamic effective grinding edge. The number of static effective grinding edges is related to the structure of the surface of the grinding wheel, while the number of dynamic effective grinding edges is also related to the movement of the grinding process.

If all feeding depth a_p is determined, the grinding grains included in the depth range will participate in the grinding work, and the description is shown in Fig. 2.

As shown in Fig. 2, multiple abrasive grains are distributed on the surface of grinding wheel, among which the highest point of abrasive grains 1#, 3#, and 6# is above 0 line. During grinding, these three abrasive grains interfere with the workpiece and will participate in cutting, so they are defined as effective abrasive grains. Other grains

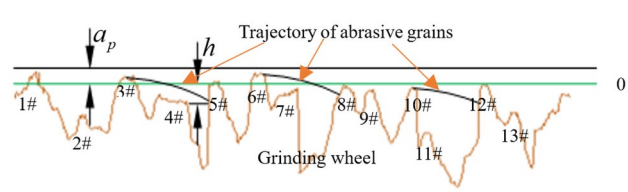

Fig. 2 Distribution of cutting edges on wheel [25]

whose highest point is below line 0 and which do not contact the workpiece are invalid (at this grinding depth).

The number of static effective grinding edges N_l per unit length can be expressed as follows [26]:

$$N_l = c_1 k_s a_p^p \tag{1}$$

where c_1 is the coefficient of grinding edge density, k_s is the coefficient of shape of abrasive grains, p is the index and $p \in (1, 2)$, and a_p is the grinding depth.

Figure 2 clearly shows the relationship between the number of static grinding edges and grinding depth. With the increase of grinding depth, the number of static grinding edges will gradually increase. However, when the number of static grinding edges reaches a certain value, its number will not change even if the grinding depth is further increased, that is because the number of grinding edges on the grinding wheel surface is limited.

Dynamic effective grinding edges are slightly different from static grinding edges. It is related to the maximum undeformed chip. In the grinding process, the undeformed chip thickness will change with the change of machining parameters. When the grinding depth is kept constant, the undeformed thickness would be increased by increasing the feed speed and decreasing the cutting speed. At this time, with the increase of the undeformed chip thickness, some grinding edges that did not participate in the original cutting will also participate in the cutting. Therefore, the abrasive grains involved in the actual grinding process are defined as dynamic effective grinding edges. It can be calculated by the following formula [25]:

$$N_\mathrm{d} = A_n C^\beta \left[\frac{v_\mathrm{w}}{v_s}\right]^\alpha \left[\frac{a_\mathrm{p}}{d_\mathrm{e}}\right]^{\alpha/2} \tag{2}$$

where A_n is the scale coefficient related to the number of static grinding edges. C is the number of abrasive grains per unit area on the surface of grinding wheel. a_p is the grinding depth. d_e is the equivalent diameter of grinding wheel. v_w is the work speed. v_s is the grinding speed. α and β respectively represent the distribution index of grinding edge on the circumference of grinding wheel.

$$\begin{cases} \alpha = \frac{p-m}{p+1} \\ \beta = \frac{p}{p+1} \end{cases} \tag{3}$$

where $P(p \in (1, 2))$ is the paternity index between N_l and a_p. m ($m \in (0, 1)$) is the index reflecting the number of grinding edges.

The number of dynamic grinding edges $N_d(l)$ within any contact length range l can be expressed as follows [27]:

$$N_d(l) = N_d\left(\frac{l}{l_c}\right)^\alpha = A_n C^\beta \left(\frac{v_w}{v_s}\right)^\alpha \left(\frac{a_p}{d_e}\right)^{\alpha/2} \left(\frac{l}{l_c}\right)^\alpha \tag{4}$$

The normal grinding force per unit contact area at a point in the contact area can be expressed as follows:

$$F_n^{'}(l) = K[A(l)]^n N_d(l) \tag{5}$$

where $A(l) = \frac{2}{A_n} C^{-\beta} \left(\frac{v_w}{v_s}\right)^{1-\alpha} \left(\frac{a_p}{d_e}\right)^{\frac{1-\alpha}{2}} \left(\frac{l}{l_c}\right)^{1-\alpha}$. K is grinding force per unit area.n $n \in (0, 1)$ is the correlation index between friction and cutting deformation. It shows that in the total grinding force, the greater the proportion of friction is, the smaller n is. Similarly, the larger n is, the greater the proportion of cutting deformation force is. When $n = 0$, it is a pure friction process. When $n = 1$, it is a pure shear process.

The grinding force per unit width is obtained by integrating $F_n^{'}(l)$ from 0 to l_c.

$$F_n^{'} = K \int_0^{l_c} A(l)^n N_d(l) dl \tag{6}$$

After simplification, the following equation is obtained [27]:

$$F_n^{'} = K C^\gamma \left(\frac{v_w}{v_s}\right)^{2\zeta-1} a_p^\zeta d_e^{1-\zeta} \tag{7}$$

where $\zeta = \frac{1}{2}[(1 + n) + \alpha(1 - n)]$, and $\gamma = \beta(1 - n)$.

2.2 Grinding force model based on experimental prediction

The factors that affect the grinding force in the grinding process are complicated. Most of the existing grinding theories are based on assumptions. The formula of grinding force derived from these grinding theories is not enough to be applied in the actual production process. Therefore, most grinding force calculation formulas used in industrial field are empirical formulas, most of which are expressed in the form of power exponential function. The commonly used method is to obtain a large number of test data through experiments, and then use regression analysis to establish empirical formulas. Generally involved in the grinding parameters mainly include grinding speed, feed speed, and grinding depth. The expression obtained by the method of multiple regression analysis is as follows:

$$F = C_\mathrm{F} v_\mathrm{s}^{a_1} v_\mathrm{w}^{a_2} a_\mathrm{p}^{a_3} \tag{8}$$

where F is grinding force (tangential grinding force F_t or normal grinding force F_n), and C_F is grinding force coefficient. a_1, a_2, and a_3 are exponential coefficients, respectively.

In addition, artificial neural network and grey prediction methods are also applied to the processing of test data. The construction method of grinding force empirical formula is

simple, the simulation accuracy is high, but its application scope is narrow. If the range of process parameters is large, a large number of tests are needed. This cost is relatively high. As the boundary conditions change, the empirical coefficient needs to be measured again, so this method is suitable for application in mass production.

3 Grinding force model based on statistics

Grinding process is a material removal process with high temperature, high strain, and high strain rate. The strain rate is generally an order of magnitude larger than that in the cutting process. The cutting dynamic mechanical properties of the workpiece material under this condition are very complex and present size effect. In most grinding force models, the coefficient of friction is used as a constant value to determine its size through grinding tests, but in fact, once the grinding process parameters change, the coefficient of friction between the grinding wheel and the workpiece also changes.

3.1 Undeformed chip analysis

The action behavior of a single abrasive and the workpiece can be characterized by the thickness of the undeformed chip. During grinding, the abrasive grains interfere with the surface of the workpiece, and the surface of the workpiece will slip and rub, marking the surface with a certain shape and size. Figure 3 shows the geometric model of grinding process, revealing the position relation between grinding wheel and workpiece and the geometric shape of undeformed grinding chip during grinding process.

Many researchers have attempted to predict the performance of grinding processes by using undeformed chip-thickness models. The undeformed chip thickness model, used to assess the performance of grinding processes, plays a major role in predicting the surface quality.

In the grinding process, the abrasive grains move in line rotation relative to the workpiece, and the closed area formed by adjacent abrasive grains in the workpiece is undeformed chip, which is the red part in Fig. 3a. The other two dotted lines are the outer contours of the grinding wheel at two moments. According to Fig. 3a, l_{AB} is the thickness of undeformed chips when the abrasive grains turn to the angle of θ. Since the grinding depth is very small compared with the diameter of the grinding wheel, angle θ and angle $\angle OBO'$ are small angles in the cutting process of the abrasive grains, so ($\angle BO'C$ and $\angle OBO'$ can be considered to be 90° ($\angle BO'C = \angle BCO' = 90°$). $\Delta CBO'$ is an isosceles triangle, so l_{AB} is equal to l_{OC} ($l_{AB} = l_{OC}$).

In $\Delta OCO'$, $l_{OC} = l_{OO'} \sin\theta$. Therefore, the thickness of the undeformed chip at the rotation angle θ can be obtained by calculating the rotation angle θ and the distance $l_{OO'}$ of the grinding wheel feed. Through the above analysis, the undeformed thickness c_θ at any position can be obtained as:

$$c_\theta = l_{OO'} \sin\theta = v_w t_\theta \sin\theta \tag{9}$$

where v_w is the feed speed of the workpiece, and t_θ is the time taken for the abrasive particle to rotate θ angle.

Theoretically speaking, the rotation angle θ of the abrasive grain can be any angle, but when considering the effective rotation angle to achieve cutting, angle θ is limited by the diameter of the accepted grinding wheel d and the grinding depth a_p. Thus, there is a maximum value θ_{max} in the abrasive cutting process. The maximum rotation angle is the final angle at which the abrasive particles are to complete the one-cycle cutting, and according to the grinding geometry the following equation holds.

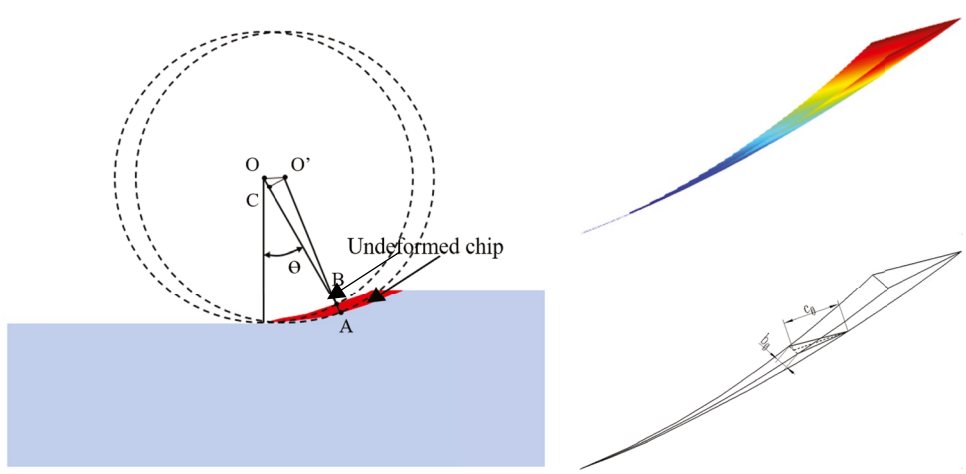

(a) Position relationship between workpiece and grinding wheel

(b) Geometry of undeformed grinding

Fig. 3 Geometric model of grinding process. **a** Position relationship between workpiece and grinding wheel. **b** Geometry of undeformed grinding

$$\sin(\theta_{\max}) = \frac{2a_{\mathrm{p}}}{l_{\mathrm{c}}} = 2\sqrt{\frac{a_{\mathrm{p}}}{d}} \tag{10}$$

where a_{p} is grinding depth, l_{c} is the contact arc length, and d is the diameter of grinding wheel.

Based on the angle $\theta_{\max}$, the maximum undeformed chip thickness $c_{\max}$ can be further obtained, and its expression is:

$$c_{\max} = h_{\max}\sin(\theta_{\max}) = 2h_{\max}\sqrt{\frac{a_p}{d}} \tag{11}$$

where $h_{\max}$ is the distance in the feed direction of the workpiece when two adjacent abrasive particles finish cutting ($h_{\max} = \frac{v_{\mathrm{w}}L}{v_s}$), and L is the distance between two abrasive grains in the circumferential direction. Substituting $h_{\max}$ into Eq. 11, the following equation can be obtained.

$$c_{\max} = \frac{2v_wL}{v_s}\sqrt{\frac{a_p}{d}} \tag{12}$$

In the grinding process, the effective rotation angle θ is small ($\sin\theta = \theta$). The undeformed chip thickness can be reduced to the following equation.

$$c_\theta = \frac{v_wL}{v_s}\theta \quad 0 \le \theta \le 2\sqrt{\frac{a_{\mathrm{p}}}{d}} \tag{13}$$

3.2 Grinding force model based on single grinding edge

The grinding force of single grinding edge is the basis of calculating and analyzing the grinding force. The tangential grinding force of a single grinding edge is the direct force that produces the cutting. It can be seen from Fig. 2 that the tangential grinding force of a single grinding edge constantly changes with the change of grinding wheel moving position and the change of undeformed chips. According to the geometry of grinding, the instantaneous cutting forces of a single grinding edge $f_{gt\theta}$ (tangential grinding force) can be expressed as follows:

$$f_{\mathrm{gt}\theta} = k_tA_{c\theta} = \frac{1}{2}k_tc_\theta b_\theta = \frac{1}{2}k_trc_\theta^2 = \frac{k_trL^2v_w^\theta\theta^2}{2v_s^2} \tag{14}$$

where θ is the rotation angle of the cutting point position of a single grinding edge. As shown in Fig. 2a, $A_{c\theta}$ is the cross-sectional area cut when the rotation angle is θ. c_θ is the thickness of undeformed chip. b_θ is the width of the undeformed chip section. As shown in Fig. 2b, r is the ratio of the width of the undeformed section to the thickness, i.e. $r = \frac{b_\theta}{c_\theta}$. k_t is the specific grinding energy (the amount of energy required to remove a unit volume of material).

In abrasive cutting, there are not only tangential forces but also normal forces. Normal grinding force $f_{gn\theta}$ can be expressed as:

$$f_{\mathrm{gn}\theta} = k_nf_{\mathrm{gt}\theta} = \frac{k_nk_trL^2v_w^2\theta^2}{2v_s^2} \tag{15}$$

where k_n is the ratio of the normal grinding force to the tangential grinding force of a single abrasive grains and $k_n = f_{gn\theta}/f_{gt\theta}$.

On the basis of obtaining the grinding forces of a single abrasive grains, the tangential grinding forces and normal grinding forces of a single abrasive grain in the coordinate system of the workpiece could be obtained through coordinate transformation. Its expression is as follows:

$$\begin{bmatrix} f_{\mathrm{g}\theta\mathrm{t}} \\ f_{\mathrm{g}\theta\mathrm{n}} \end{bmatrix} = \begin{bmatrix} \cos\theta & \sin\theta \\ \sin\theta & \cos\theta \end{bmatrix} \begin{bmatrix} f_{gt\theta} \\ f_{gn\theta} \end{bmatrix} \tag{16}$$

In the grinding process, because θ is very small, there are $\sin\theta = \theta$ and $\cos\theta = \sqrt{1-\theta^2}$. Equation 16 can be simplified as:

$$\begin{cases} f_{\mathrm{g}\theta\mathrm{t}} = \frac{k_trL^2v_w^2\theta^2}{2v_s^2}(\sqrt{1-\theta^2} + k_n\theta) \\ f_{\mathrm{g}\theta\mathrm{n}} = \frac{k_trL^2v_w^2\theta^2}{2v_s^2}(\theta + k_n\sqrt{1-\theta^2}) \end{cases} \tag{17}$$

where L is the distance between adjacent abrasive grains. When calculating grinding force, the surface parameters of the test grinding wheel can be obtained by measuring the surface topography of the grinding wheel.

3.3 Grinding force calculation based on statistics

In grinding, for effective abrasive grains, the size of cutting angle directly affects the thickness of undeformed chip and the size of grinding force. Therefore, the cutting angle of a single abrasive particle should be known first when calculating the grinding force. The cutting angle of any effective abrasive grain can be expressed as:

$$\theta_j = \frac{v_st_{j,0}}{d} \tag{18}$$

where $t_{j,0}$ is the relative time of abrasive cutting, and $t_{j,0} = floor\left(\frac{\sum L_{i+1}+L_{i+2}+\cdots L_{i+n}}{v_s\Delta t}\right)\cdot\Delta t + \lambda\Delta t$. where function "*floor*" is rounded to the left, $0 \le \lambda < floor(\frac{L_{i+n+1}}{v_s\Delta t})$, and $\lambda \in N$. In addition, there are the following equations.

$$\begin{cases} t_{j,0} = floor\left(\frac{\sum L_{i+1}+L_{i+2}+\cdots L_{i+n}}{v_s\Delta t}\right)\cdot\Delta t + \lambda\Delta t \\ t_{j+1,0} = floor\left(\frac{\sum L_{i+2}+L_{i+3}+\cdots L_{i+n}}{v_s\Delta t}\right)\cdot\Delta t + \lambda\Delta t \\ \vdots \\ t_{j+n-1,0} = floor\left(\frac{L_{i+n}}{v_s\Delta t}\right)\cdot\Delta t + \lambda\Delta t \\ t_{j+n,0} = \lambda\Delta t \end{cases} \tag{19}$$

The tangential grinding force of No. i abrasive grain at time t_0 can be obtained by substituting Eq. 18 into Eq. 17, and its expression is as follow:

$$f_{g_i\theta_j t_0} = \frac{k_t r L_i^2 v_w^2 t_{j,0}^2}{2d^2}\left(\sqrt{1-\frac{v_s t_{j,0}^2}{d^2}} + k_n \frac{v_s t_{j,0}}{d}\right) \tag{20}$$

On this basis, the tangential grinding force ($f_{g_i\theta_j t_k}$) of No. i abrasive particle at any time can be further calculated.

$$f_{g_i\theta_j t_k} = \frac{k_t r L_i^2 v_w^2 (t_{j,0}+k\Delta t)^2}{2d^2}\left(\sqrt{1-\frac{v_s (t_{j,0}+k\Delta t)^2}{d^2}} + k_n \frac{v_s (t_{j,0}+k\Delta t)}{d}\right) \tag{21}$$

In the grinding process, with the increase of the cutting angle of the abrasive particles, the abrasive particles gradually separated from the workpiece. When the abrasive particles are beyond the workpiece, the grinding force disappeared. So there is a constraint on k. In the general case, $k < floor(\sqrt{a_p d}/v_s - t_{j,0})$, if $k > floor(\sqrt{a_p d}/v_s - t_{j,0})$, then $i = i + 1$. In addition, when $\lambda + k \geq floor(\frac{L_{i+n+1}}{v_s \Delta t})$, then $n = n + 1$ and $\lambda = \lambda + k - floor(\frac{L_{i+n+1}}{v_s \Delta t})$.

In the grinding process, there are many abrasives involved in cutting. Taking a single row of abrasives as an example, all abrasives at the contact arc length may participate in cutting. Therefore, the single-row grinding force of the grinding wheel can be expressed as:

$$F_{\mathrm{tk}} = \sum f_{g_i\theta_j t_k} + f_{g_{i+1}\theta_{j+1} t_k} + \cdots f_{g_{i+n}\theta_{j+n} t_k} \tag{22}$$

On the basis of Eq. 22, grinding force per unit width can be obtained by further calculation, which is expressed as:

$$\begin{cases} F_t = \frac{F_{tk}}{\overline{\mathrm{L}}} = \frac{\sum f_{gi}\theta_j t_k + f_{g_i+1}\theta_{j+1} t_k + \cdots f_{gi+n}\theta_{j+n^t} k_{tk}}{\overline{\mathrm{L}}} \\ F_n = \frac{k_n F_{tk}}{\overline{\mathrm{L}}} = \frac{k_n \sum f_{gi}\theta_j t_k + f_{g_i+1}\theta_{j+1} t_k + \cdots f_{gi+n}\theta_{j+n^t} k_{tk}}{\overline{\mathrm{L}}} \end{cases} \tag{23}$$

where $\overline{L}$ is the average spacing of abrasive grains.

4 Grinding force calculation and experiment setup

4.1 Parameter estimation of grinding wheel

In order to further understand the distribution of abrasive grains on the surface of grinding wheel, the CBN grinding wheel with grain size of 120/140# and concentration of 100% was taken as the research object, and its surface morphology was tested. In order to facilitate the test, the prepared grinding wheel was crushed, 10 sample blocks were randomly selected, the surface of the grinding wheel was photographed by scanning electron microscope, and 20 morphology photos under 500× were selected. The calibration was carried out by Cooling Tech software and the test of abrasive spacing was completed. After statistical analysis, the mean value and standard deviation are calculated ($\bar{x} = 123.96\mu$m, and $s = 29.91\mu$m). It is assumed that the spacing of abrasive grains follows a normal distribution, and the fitting result is shown in Fig. 4b.

For further verification, it is necessary to test whether the abrasive spacing obeyed the proper distribution (hypothesis testing). According to the nature of the problem, hypothesis testing mainly includes parametric testing and

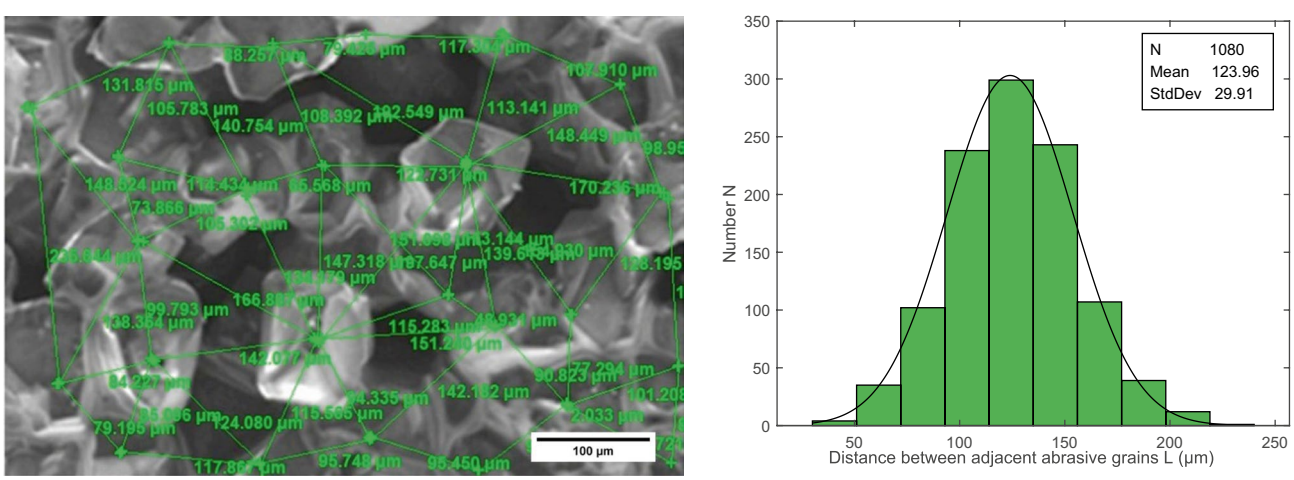

(a) Measurement of distance between two adjacent abrasive grains

(b) Statistics of distance between adjacent abrasive grains

Fig. 4 Distance analysis of adjacent CBN abrasive grains. **a** Measurement of distance between two adjacent abrasive grains. **b** Statistics of distance between adjacent abrasive grains

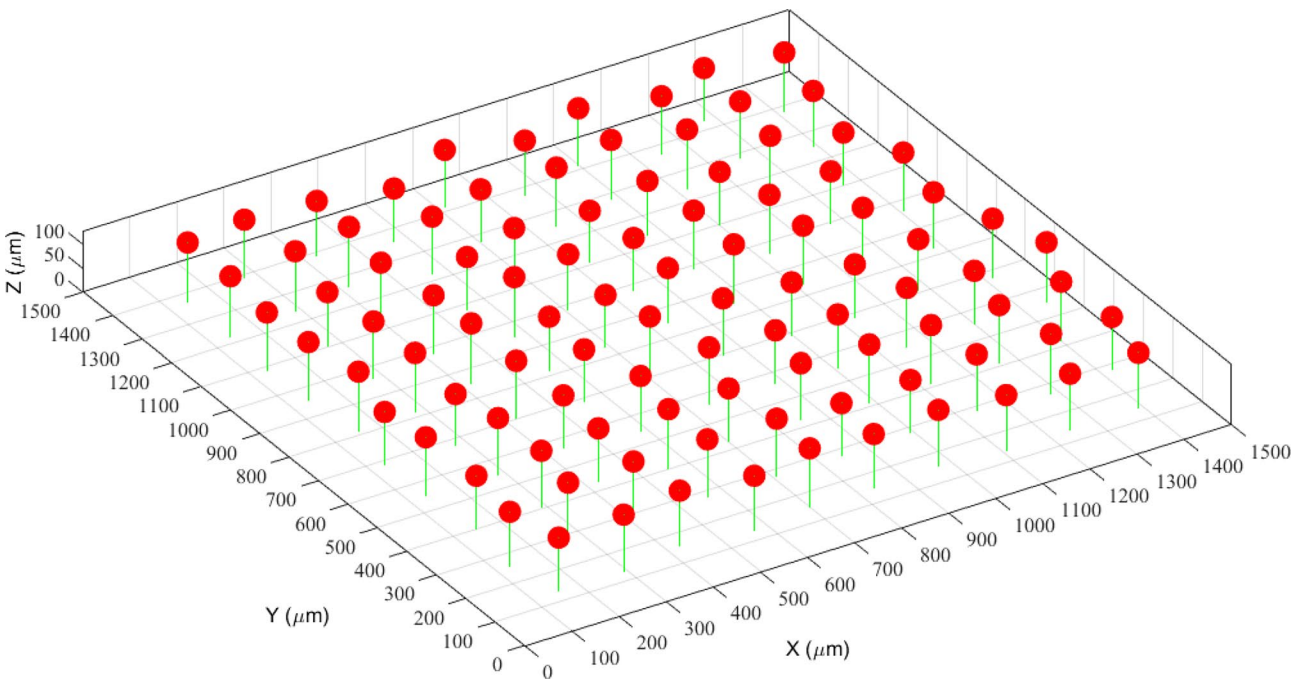

Fig. 5 Distribution of abrasive grains

nonparametric testing. For the problem of abrasive spacing, its distribution function has been fitted and approximated to follow the normal distribution, so it only needs to carry out parameter test.

Abrasive spacing L follows the normal distribution of $N(\mu, \sigma^2)$. μ and σ can be estimated from the sample.

$$\begin{cases} \mu = \overline{x} \\ \sigma = s \end{cases} \tag{24}$$

where $\overline{x}$ and s are the sample mean and standard deviation, respectively. The confidence intervals$(100(1-\alpha)\%)$ for μ and σ^2 are as follows [28]:

$$\begin{cases} \left(\overline{x} - t_{1-\frac{\alpha}{2}}(n-1)\frac{S}{\sqrt{n}}, \overline{x} + t_{1-\frac{\alpha}{2}}(n-1)\frac{S}{\sqrt{n}}\right) \\ \left(\frac{(n-1)S^2}{\chi^2_{1-\frac{\alpha}{2}}(n-1)}, \frac{(n-1)S^2}{\chi^2_{\frac{\alpha}{2}}(n-1)}\right) \end{cases} \tag{25}$$

If $\alpha = 0.05$, $t_{0.975}(1079) = 1.96$, $\chi^2_{0.025}(1079) = 989.87$, and $\chi^2_{0.975}(1079) = 1171.93$. On this basis, the confidence interval with 95% confidence probability of mean μ and standard deviation σ can be obtained, respectively, as $[122.1761, 125.7439]$ and $[28.6988, 31.2255]$. Therefore, it could be determined that the spacing of abrasive grains approximately obeyed the proper distribution, so its probability density function could be expressed as:

$$f = \frac{1}{\sqrt{2\pi\sigma}}\exp(-\frac{\mu^2}{2\sigma^2}) \tag{26}$$

where $\mu = 123.96\mu$m and $\sigma = 29.91\mu$m.

Assuming that only half of the abrasive grains on the surface of the grinding wheel are exposed, the height of the abrasive grains on the surface of the grinding wheel is the half height of the abrasive grains. Using the mean value and standard deviation of the measured distribution of abrasive grains, the spatial distribution of abrasive grains was obtained, and it was shown in Fig. 5.

4.2 Calculation of cutting force coefficient (grinding specific energy)

The grain size of the ceramic CBN sample block used in the test was the same as that of the test grinding wheel, which was 120/140#. The grinding specimen was a semi-cylindrical insert, which is fixed on the disc during the test, and the ceramic CBN sample block was held by flat pliers. In the grinding process, the specimen rotated with the spindle, and the grinding test of a single abrasive grain would be completed by adjusting the relative distance between the ceramic CBN sample block and the specimen. The test platform and test parameters are shown, respectively, in Fig. 6 and Table 1.

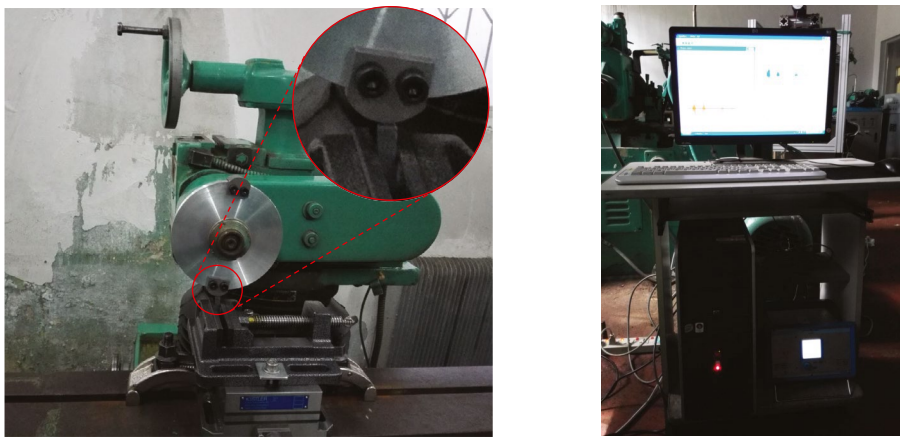

(a) Grinding test of single grain **(b)** Grinding force acquisition and processing unit

Fig. 6 Grinding force test platform for single grain. **a** Grinding test of single grain. **b** Grinding force acquisition and processing unit

The test device for the grinding of vitrified CBN ceramic CBN sample block is shown in Fig. 6a. During the test, the position of the ceramic CBN sample block was fixed, while the specimen rotated at a linear speed of 20 m/s. The single grain grinding test was completed under dry grinding conditions. During the test, the contact zero point between the most prominent abrasive grain and the specimen was found by means of trial cutting. Then, changing the cutting position of the ceramic CBN sample block along the axial direction and setting the grinding depth, the single grain grinding would be completed. The corresponding grinding force was recorded by a dynamometer, and eventually scores were left on the cambered surface of the specimen, as shown in Fig. 7a. In order to calculate the cutting coefficient of abrasive grains, the most prominent notch in the grinding process was selected to correspond with the maximum grinding force. The cutting cross section of a single abrasive grain and the corresponding grinding force are shown, respectively, in Figs. 7b and 8. And the 3D surface morphology was measured by confocal laser microscope.

Under the premise that the grinding cross section and tangential grinding forces of a single abrasive particle are known, the grinding force coefficient (grinding specific energy $k_t = \frac{F_x}{A_c} = \frac{11.52}{132.56\times50/2} \times 10^{12} = 3476\text{J/mm}^3(3.476\text{GPa}))$ can be calculated by Eq. 14. The grinding force coefficient k_t and grinding force ratio k_n calculated by the test were brought into the statistical grinding force model, and the grinding force under the same test parameters was calculated. The results are shown in Fig. 9.

Grinding specific energy under different grinding parameters is not nearly the same. And the undeformed chip thickness has been broadly utilized to better understand the grinding mechanism and the Specific energy. Therefore, by adjusting the relative distance between the ceramic CBN sample block and the test block, the undeformed chip thickness could be changed. And the specific grinding energy under corresponding undeformed chip thickness was calculated. The results were shown in Fig. 10. When the deformation cutting thickness was less than 20 μm, the specific energy decreased sharply with the increase of the undeformed chip thickness. When the undeformed chip thickness was 20–40 μm, the specific energy decreases slowly with the increase of the deformation cutting thickness. When the undeformed chip thickness was greater than 50 μm, with the increase of the cutting thickness for deformation, the grinding specific energy was almost unchanged and tended to be stable at 3460 J/mm^3.

Table 1 Grinding parameters of single abrasive grain

Grinding parameter	Value
Grinding speed v_s	20 m/s
Grinding depth a_p	50 μm
Rotary radius of grinding specimen r	70mm
Diameter of grinding specimen d	30mm
Grinding conditions	Dry grinding
Material	45G

4.3 Influence of grinding parameters on grinding forces

On the basis of single abrasive grain grinding test, in order to further verify the correctness of statistical grinding force model, the grinding force of CBN wheel with vitrified bond was measured by Kistler dynamometer (9257BA). The test platform is shown in Fig. 11, and the grinding conditions and machining parameters are shown in Table 2.

Fig. 7 Grinding surface topography of single abrasive. **a** Grinding the surface with a single abrasive (). b Grinding cross section

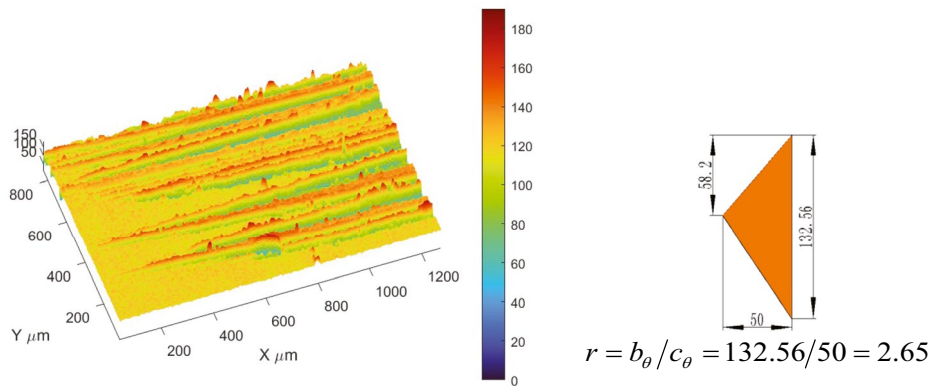

(a) Grinding the surface with a single abrasive ($a_p = 50\mu m$)

(b) Grinding cross section

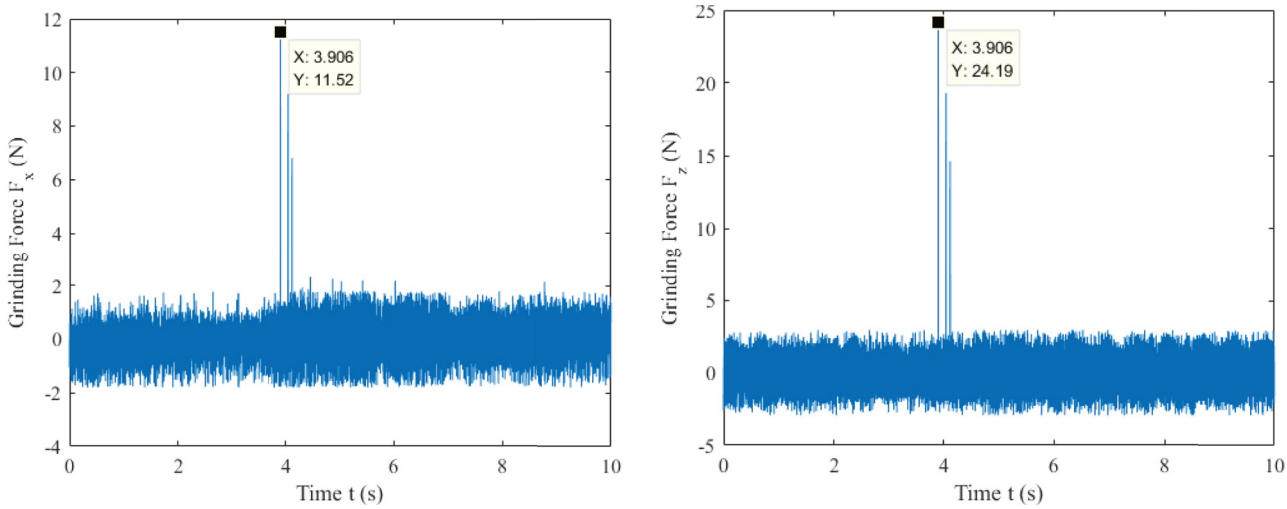

(a) Tangential grinding force

(b) Normal grinding force

Fig. 8 Grinding force of single abrasive (grinding force ratio k_n = F_z/F_x = 24.19/11.52 = 2.10). **a** Tangential grinding force. **b** Normal grinding force

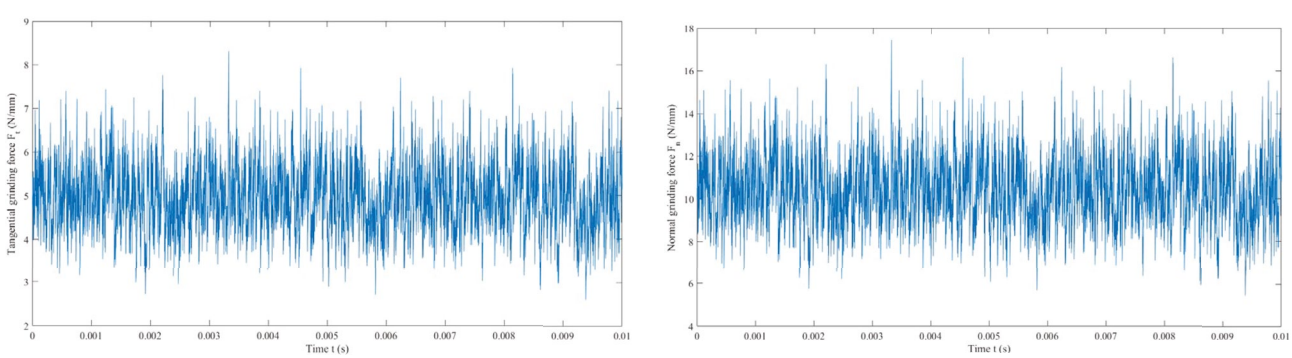

(a) Tangential grinding force

(b) Normal grinding force

Fig. 9 Statistics grinding force (v_s = 20"m/s," v_"w" = 0.2"m/min," a_"p" = 50"μm," k_t = 3476"J"/〖"mm" 〗^3). **a** Tangential grinding force. **b** Normal grinding force

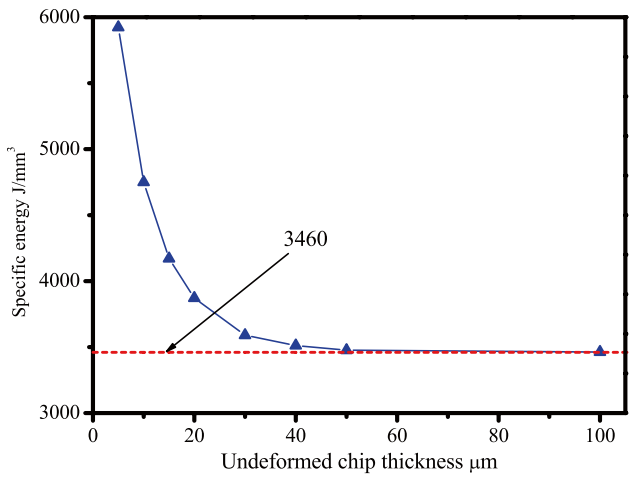

Fig. 10 Specific energy change law with the change of undeformed chip thickness

4.3.1 (1) Influence of grinding depth on grinding force

Grinding depth is an important parameter to determine the relative position relationship between grinding wheel and specimen. Generally speaking, the grinding force will gradually increase with the increase of grinding depth, but the value of grinding force and its change rule also have a great relationship with the performance of grinding wheel and material properties. Figure 12 shows the comparison of instantaneous calculated tangential grinding forces and experimental tangential grinding forces at different grinding depths. Figure 12 shows the average values of calculated and tested tangential grinding forces at different grinding depths.

It can be seen from Figs. 12 and 13 that the calculated grinding force and the test grinding force have basically the same variation trend. With the increase of grinding depth, the grinding force gradually increases and shows a superlinear growth. However, with the increase of grinding depth, the difference between them gradually increases. There are two main reasons. The first point was that the interference of axial distributed abrasive grains during cutting was not considered in the grinding force mode. However, with the increase of grinding depth, the cutting cross sections between the axial adjacent abrasive grains may overlap, but the overlapping part was not removed when calculating the grinding force. Therefore, the calculated value was larger than the measured value. The second point was caused by the stiffness of the machine tool itself. With the increase of grinding depth, the normal grinding force would also increase. Under the action of the larger normal force, the machine tool spindle would produce a small bending deformation, which would cause the actual grinding depth to be less than the set grinding depth.

Table 2 Grinding test conditions and processing parameters

Grinding parameter	Value
Grinding conditions	Down grinding (No grinding fluid)
Grinding wheel	P 200 × 10 × 32 CBN 120 VJ100
Grinding specimen mm	45G 60×20×25
Grinding speed v_s (m/s)	20, 25, 30, 35
Feed speed v_w (m/min)	1, 2, 3, 4, 5
Grinding depth a_p (μm)	10, 20, 30

4.3.2 (2) Influence of feed speed on grinding force

Feed is the basis of continuous grinding. Under the premise of constant grinding speed, the thickness of undeformed chip will increase with the increasing of feed speed, and the material removal amount per unit time is also increased. From the perspective of grinding kinematics and energy, the grinding force will be significantly increased with the increase of workpiece feed speed. Figure 14 shows the instantaneous values of calculated grinding forces and test grinding forces

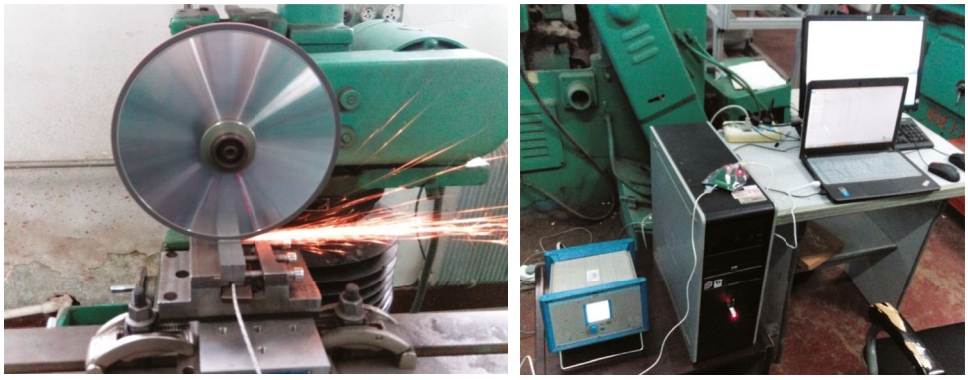

(a) Grinding test **(b)** Grinding force acquisition and processing system

Fig. 11 Grinding test platform. **a** Grinding test. **b** Grinding force acquisition and processing system

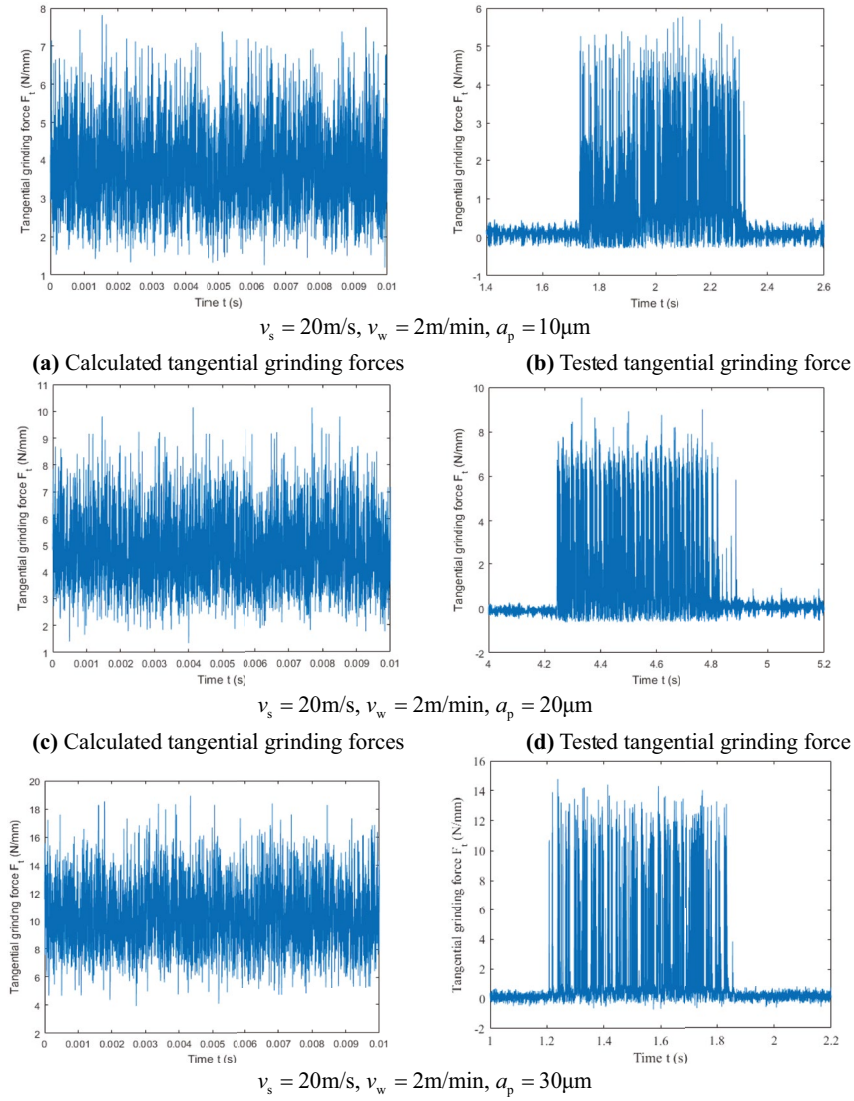

Fig. 12 Tangential grinding force under different grinding depths. **a** Calculated tangential grinding forces. **b** Tested tangential grinding force. **c** Calculated tangential grinding forces. **d** Tested tangential grinding force. **e** Calculated tangential grinding forces. **f** Tested tangential grinding force

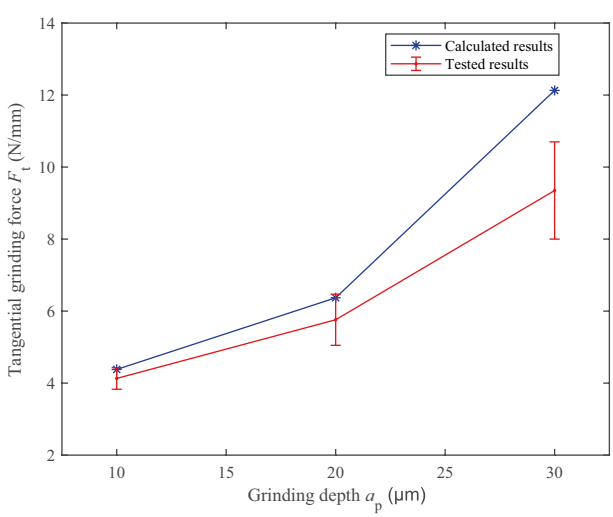

Fig. 13 Changing rule of tangential grinding force with changing of grinding depths

at different feed speeds. Figure 15 shows the average values of calculated grinding forces and test grinding forces at different feed speeds.

As shown in Figs. 14 and 15, the feed speed has a significant effect on the tangential grinding force. The calculated tangential grinding force is similar to the experimental tangential grinding force, and the fluctuation range of instantaneous grinding force increases. The tangential grinding force increases linearly. This is due to the increase of feed speed, so that the uneven distribution of abrasive grains on the tangential grinding force becomes more significant. In addition, the difference between the calculated tangential grinding forces and the experimental tangential grinding forces increases with the increase of the workpiece feed speed. The main reason for the error between the calculated value and the test value is that the increase of the feed speed makes the tangential grinding force and the normal grinding

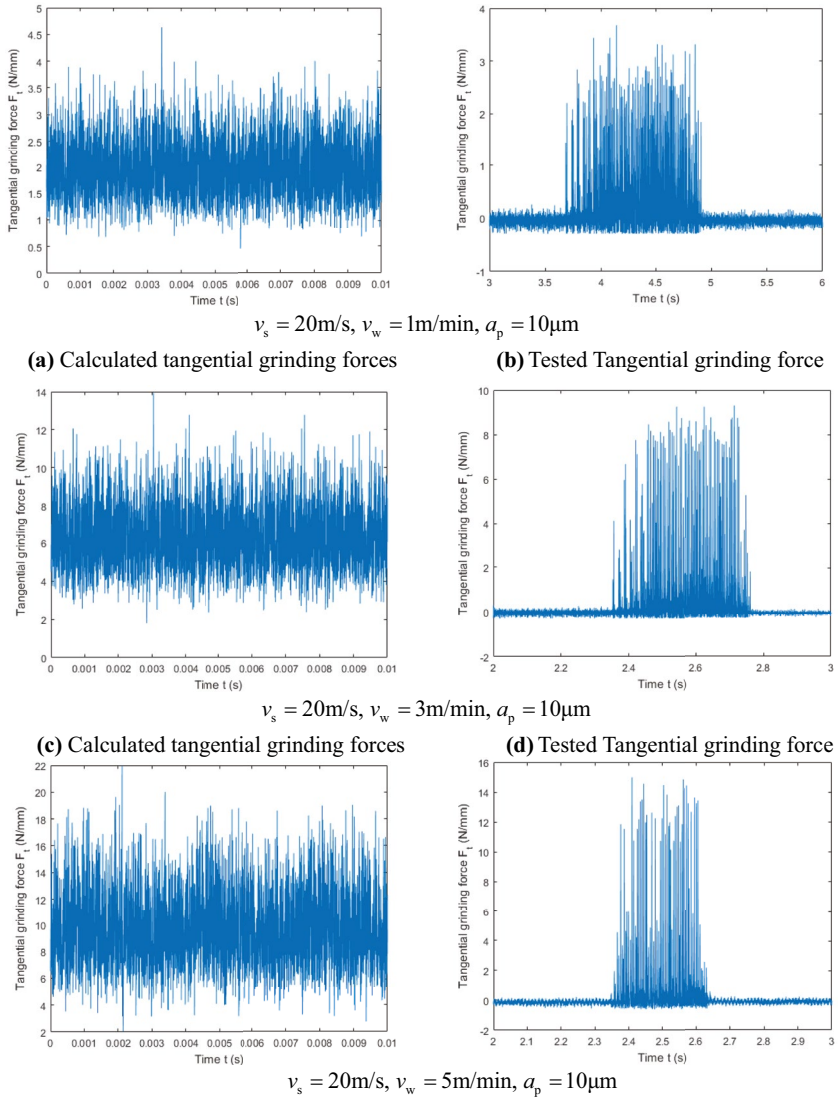

Fig. 14 Tangential grinding force under different feeding speed. **a** Calculated tangential grinding forces. **b** Tested Tangential grinding force. **c** Calculated tangential grinding forces. **d** Tested Tangential grinding force. **e** Calculated tangential grinding forces. **f** Tested Tangential grinding force

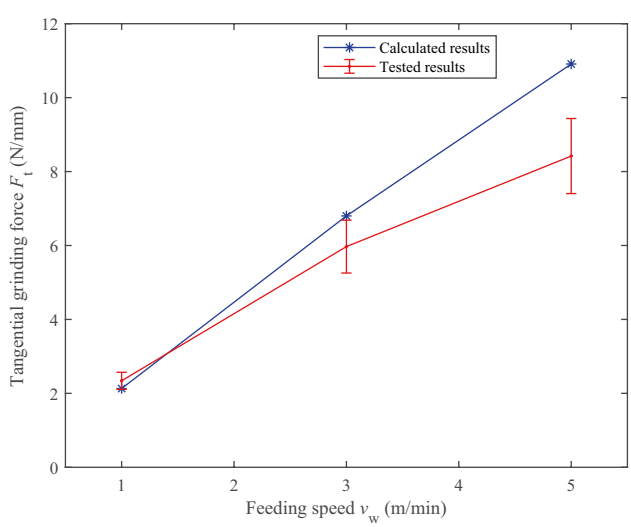

Fig. 15 Variation of tangential grinding force with feed speed

force increase to a certain extent. Due to the influence of the spindle stiffness, the actual grinding depth decreases with the increase of the workpiece feed speed, so that the difference between them increases with the increase of the workpiece feed speed.

4.3.3 (3) Influence of grinding speed on grinding force

Grinding speed is also an important parameter affecting grinding force. The size of grinding speed has a certain influence on grinding force and quality. With the increase of grinding speed, the thickness of undeformed chip will decrease, and the number of effective cutting edges per unit time will significantly increase. From the perspective of energy, since the feed speed of the workpiece remains unchanged, the amount of material removed by the grinding wheel per unit time basically remains unchanged. In view of

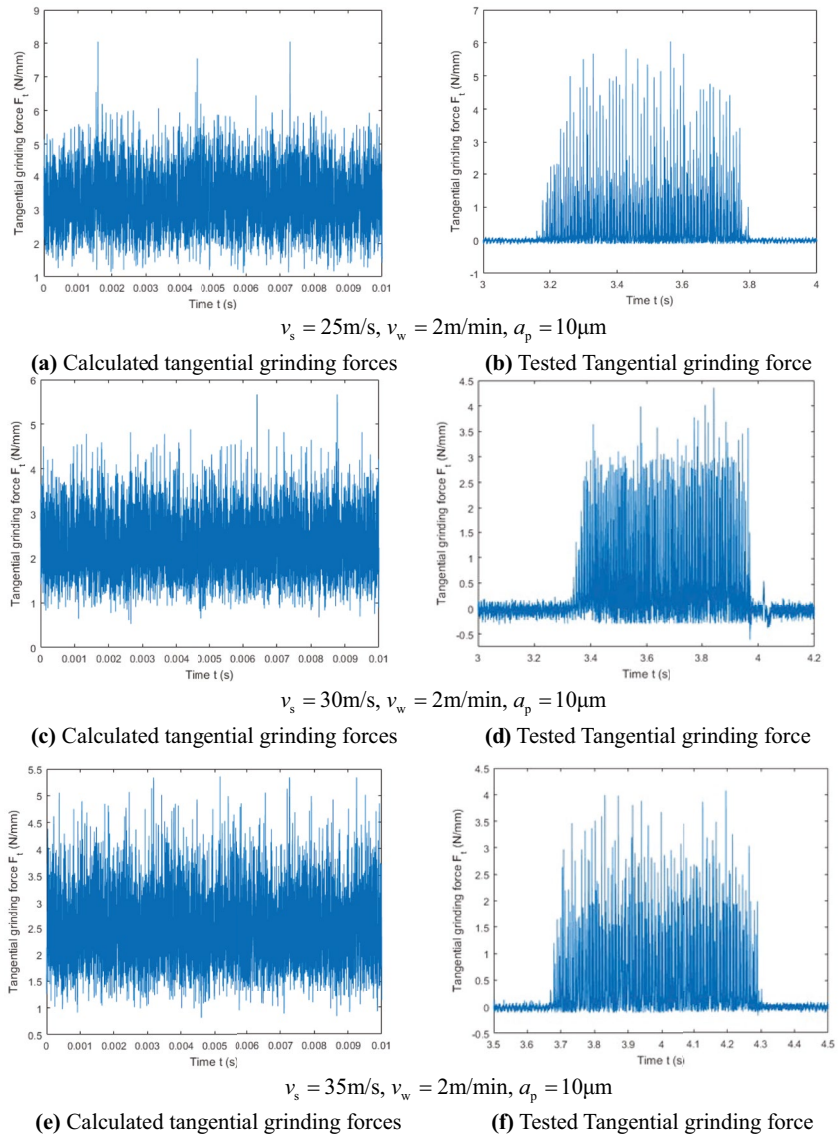

Fig. 16 Tangential grinding force under different grinding speed. **a** Calculated tangential grinding forces. **b** Tested Tangential grinding force. **c** Calculated tangential grinding forces. **d** Tested Tangential grinding force. **e** Calculated tangential grinding forces. **f** Tested Tangential grinding force

this, it can be considered that the consumption of grinding energy per unit time is approximately unchanged, because the consumption of grinding energy is mainly reflected as the product of grinding speed and tangential grinding force. Therefore, on the premise of keeping other grinding parameters unchanged, the grinding force will be reduced by increasing grinding speed. Figure 16 shows the instantaneous values of calculated grinding forces and test grinding forces at different grinding speeds. Figure 17 shows the average values of calculated grinding forces and test grinding forces at different grinding speeds.

Figures 16 and 17 show that the tangential grinding force decreases with the increase of grinding speed, but the rate of change gradually decreases. At the same time, the difference between the two is gradually widening. The reason is that the grinding force coefficient (specific grinding energy) decreases with the increase of grinding speed, which reduces

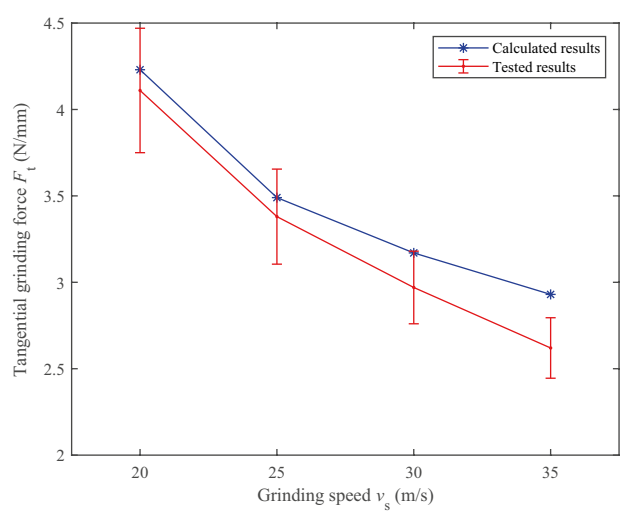

Fig. 17 Tangential grinding force changing with changing of grinding speed

the friction coefficient between the abrasive grains and the workpiece.

Specific grinding energy is an important characterization of grinding wheel. Its physical meaning is the energy consumed to remove the unit volume of material. Specific grinding energy is related to the characteristics of grinding wheel, material properties, and grinding processing parameters. And its value is related to the structure of grinding wheel, material type, and actual cutting parameters. The calculation of specific grinding energy by single grain grinding test was not very comprehensive. And, the specific grinding energy will change slightly with the change of grinding parameters, which is also the reason for the difference between these two grinding forces.

5 Conclusion

In this paper, based on the characteristics of grain orientation of CBN grinding wheel with vitrified bond and undeformed chips, the statistical grinding force model with dynamic grinding edges was established considering the random distribution of abrasive particles on the surface of grinding wheel. The model was verified by grinding 45 steel with vitrified bonded CBN grinding wheel. The main conclusions are as follows:

Grinding specific energy decreased with the increase of the undeformed chip thickness. When the undeformed chip thickness was less than 20 μm, the grinding specific energy decreased sharply with the increasing of the undeformed chip thickness. When the undeformed chip thickness was more than 50 μm, the grinding specific energy almost unchanged and tended to be stable at 3460 J/mm^3.

The statistical grinding force model can display the changing process of grinding force in real time, reveal the mechanism of abrasive particle discontinuous cutting in the grinding process, and effectively predict grinding force.

The statistical grinding force model can reflect the real value of grinding force to a certain extent. The model has good applicability for small cutting depth, slow feed, and low speed models. With the increasing of grinding depth, feed speed, and grinding speed, the gap between the calculated grinding force and the test value gradually increased.

The variation trend of the calculated grinding force was basically the same as that of the test grinding force. With the increase of grinding depth, the grinding force gradually increased and showed a superlinear growth. With the increasing of workpiece feed speed, the fluctuation range of instantaneous grinding force increased, and the tangential grinding force increased linearly. With the increasing of grinding speed, the tangential grinding force decreased, but the smaller grinding speed gradually decreased.

Author contribution Methodology, formal analysis, investigation, data curation, writing-original draft: Xuezhi Wang; writing-review and editing, supervision: Qingyao Liu; writing-review and editing, supervision: Yaohui Zheng; writing-review and editing, supervision: Wei Xing; methodology: Minghai Wang.

Funding This research is supported by the Natural Science Foundation of Liaoning Province (No. 2021-MS-263), Open Fund of Key Laboratory of Fundamental Science for National Defense of Aeronautical Digital Manufacturing Process of Shenyang Aerospace University (SHSYS-202101), Foundation of Liaoning Province Education Administration (NO. JYT 2020132), and Independent Innovation Special Fund Project of AECC (ZZCX-2019–019).

Data availability Data will be available upon request.

Declarations

Ethical approval Not applicable.

Consent to participate Not applicable.

Consent to publish Not applicable.

Conflict of interest The authors declare no competing interests.

References

1. Cao J et al (2015) A grinding force model for ultrasonic assisted internal grinding (UAIG) of SiC ceramics. J Adv Manuf 81(5–8):875–885
2. Dai C et al (2019) Grinding force and energy modeling of textured monolayer CBN wheels considering undeformed chip thickness nonuniformity. Int J Mech Sci 157–158:221–230
3. Huang S, Yu X (2017) A study of grinding forces of SiCp/Al composites. J Adv Manuf 94(9–12):3633–3639
4. Fuh K, Wang S (1997) Force modeling and forecasting in creep feed grinding using improved bp neural network. Int J Mach Tools Manuf 37(8):1167–1178
5. Gu P et al (2020) A grinding force prediction model for SiCp/Al composite based on single-abrasive-grain grinding. J Adv Manuf 109(5–6):1563–1581
6. Guo Y, Liu M, Li C (2020) Modeling and experimental investigation on grinding force for advanced ceramics with different removal modes. J Adv Manuf 106(11–12):5483–5495
7. Duan N et al (2017) SPH and FE coupled 3D simulation of monocrystal SiC scratching by single diamond grit. Int J Refract Metal Hard Mater 64:279–293
8. Setti D, Kirsch B, Aurich JC (2017) An analytical method for prediction of material deformation behavior in grinding using single grit analogy. Procedia CIRP 58:263–268
9. Chang H-C, Wang JJJ (2008) A stochastic grinding force model considering random grit distribution. Int J Mach Tools Manuf 48(12–13):1335–1344
10. Hecker RL, Ramoneda IM, Liang SY (2003) Analysis of wheel topography and grit force for grinding process modeling. J Manuf Process 5(1):13–23
11. Hecker RL et al (2006) Grinding force and power modeling based on chip thickness analysis. J Adv Manuf 33(5–6):449–459
12. Liu Y, Li B, Wu C et al (2016) Simulation-based evaluation of surface micro-cracks and fracture toughness in high-speed grinding of silicon carbide ceramics[J]. Int J Adv Manuf Technol 86:799–808

13. Guizhi X et al (2011) Grinding force modeling for high-speed deep grinding of engineering ceramics [J]. J Mech Engine 2011, 47(11):169–169
14. Shao Y et al (2015) Physics-based analysis of minimum quantity lubrication grinding. J Adv Manuf 79(9–12):1659–1670
15. Zhang Y, Li C, Ji H, Yang X, Yang M, Jia D, Zhang X, Li R, Wang J (2017) Analysis of grinding mechanics and improved predictive force model based on material-removal and plastic-stacking mechanisms. Int J Mach Tools Manuf 122:81–97
16. Zhang D et al (2015) Specific grinding energy and surface roughness of nanoparticle jet minimum quantity lubrication in grinding. Chin J Aeronaut 28(2):570–581
17. Cheng J et al (2015) Study on grinding force modelling and ductile regime propelling technology in micro drill-grinding of hard-brittle materials. J Mater Process Technol 223:150–163
18. Zhang X et al (2019) Grinding force modelling for ductile-brittle transition in laser macro-micro-structured grinding of zirconia ceramics. Ceram Int 45(15):18487–18500
19. Li HN et al (2017) Detailed modeling of cutting forces in grinding process considering variable stages of grain-workpiece micro interactions. Int J Mech Sci 126:319–339
20. Zahedi A, Tawakoli T, Akbari J (2015) Energy aspects and workpiece surface characteristics in ultrasonic-assisted cylindrical grinding of alumina–zirconia ceramics. Int J Mach Tools Manuf 90:16–28
21. Zhou M, Zheng W (2016) A model for grinding forces prediction in ultrasonic vibration assisted grinding of SiCp/Al composites. J Adv Manuf 87(9–12):3211–3224
22. Gu KK et al (2015) Analysis on the effects of rotational speed of grinding stone on removal behavior of rail material. Wear 342–343:52–59
23. Tian L et al (2015) The influence of speed on material removal mechanism in high speed grinding with single grit. Int J Mach Tools Manuf 89:192–201
24. Ding W et al (2017) Grinding performance of textured monolayer CBN wheels: undeformed chip thickness nonuniformity modeling and ground surface topography prediction. Int J Mach Tools Manuf 122:66–80
25. Chong S (2009) Research on Key and Technologies of Virtual Grinding. Northeastern University
26. Bo LBZ (2003) Modern grinding technology. China Machine Press, Beijing
27. Yongping C (2007) Research on modeling and application of surface grinding force. Central South University 22–23
28. Rongheng S (2014) Applied Mathematical Statistics. Science press, Beijing

Publisher's Note Springer Nature remains neutral with regard to jurisdictional claims in published maps and institutional affiliations.